Journal of Biomedical Optics

BiomedicalOptics.SPIEDigitalLibrary.org

Label-free nonenzymatic glycation monitoring of collagen scaffolds in type 2 diabetic mice by confocal Raman microspectroscopy

Panpan Shi
Hanping Liu
Xiaoyuan Deng
Ying Jin
Qiannan Wang
Hao Liu
Maosheng Chen
Xue Han

SPIE.

Label-free nonenzymatic glycation monitoring of collagen scaffolds in type 2 diabetic mice by confocal Raman microspectroscopy

Panpan Shi, Hanping Liu,* Xiaoyuan Deng, Ying Jin, Qiannan Wang, Hao Liu, Maosheng Chen, and Xue Han
South China Normal University, College of Biophotonics, No. 55 Zhongshan Avenue West, Tianhe District, Guangzhou 510631, China

Abstract. Collagen is the key target of nonenzymatic glycation during physiopathological processes such as diabetes. The induced changes in the biochemical property of collagen by nonenzymatic glycation remain a major challenge to probe. This study investigated the use of confocal Raman microspectroscopy to label-free monitor the nonenzymatic glycation of collagen scaffolds from type 2 diabetic (T2D) mice at different timepoints (0, 4, 8, and 12 weeks). The glycated collagen scaffolds were obtained through the decellularized dermal matrix method to remove the epidermis layer, subcutaneous tissue, and cells in the dermis and to retain the collagen fibrils. Raman spectra showed no changes in Raman peak positions, which indicated that nonenzymatic glycation could produce no significant changes in the triple-helix structure of collagen in T2D mice. However, the relative intensity of the Raman bands at 921, 1033, 1244, 1274, 1346, 1635, and 1672 cm^{-1} increased as diabetic time progressed. Correlation analysis suggested that the spectra of these bands had a high positive correlation with the expression of anti-advanced glycation end products obtained by immunofluorescence imaging of the same collagen scaffolds. Confocal Raman microspectroscopy proves a potential tool to label-free monitor the collagen changes caused by nonenzymatic glycation in T2D mice. [DOI: 10.1117/1.JBO.20.2.027002]

Keywords: type 2 diabetes; nonenzymatic glycation; advanced glycation end products; decellularized dermal matrix; collagen scaffolds; confocal Raman microspectroscopy.

Paper 140694R received Oct. 22, 2014; accepted for publication Jan. 13, 2015; published online Feb. 11, 2015.

1 Introduction

Diabetes is a disorder of chronic hyperglycemia (high glucose in blood) and is commonly subdivided into two prevalent types, namely, type 1 diabetes and type 2 diabetes (T2D).[1] T2D is characterized by insulin resistance or the relative lack of insulin.[2] This predominant type accounts 90% to 95% of individuals and is the noninsulin-dependent diabetes or adult-onset diabetes.[3] Chronic hyperglycemia in diabetes can cause long-term damage, dysfunction, and failure of different organs, especially the eyes, kidneys, nerves, heart, and blood vessels, as well as the skin.[4]

Protein glycation reactions that lead to the formation of advanced glycation end products (AGEs) are the major causes of different diabetic complications.[5] Protein glycation initiated by spontaneous nonenzymatic reactions between free amino groups of long-life proteins and carbonyl groups of reducing sugars first forms reversible Schiff bases, which subsequently undergo Amadori rearrangement leading to stable ketoamine bonds.[6] Further oxidation, dehydration, and cross-linking steps induce the generation of compounds. These compounds exhibit significantly enhanced reactivity for sites, such as arginine and lysine residues on proteins, resulting in the formation of AGEs. The formation of AGEs results in poorly characterized heterogeneous products which are linked in a complicated network.[7] High glucose levels in diabetes can easily induce the glycation of various structural and functional proteins, including plasma proteins and collagen.[8]

Collagen is the longest living protein and a major component of the extracellular matrix; this protein is a well-characterized natural material with multiple levels of structural order.[9] Thus, collagen is a prominent target of nonenzymatic glycation.[10] In a diabetic body, collagen is continuously exposed to high glucose in vascular and extravascular fluids. AGEs alter the collagen properties, such as by losing the triple helix solubility and flexibility, and thus increase its rigidity.[11] Cross-linked collagen contributes to diabetes complications, especially diabetic dermopathy. One-third of people with diabetes have an associated skin disease at some time in their lives.[12] Collagen glycation augments the formation and migration of myofibroblasts and participates in the development of fibrosis in diabetes.[13] Increasing evidence indicates that the excess accumulation of collagen AGEs in the diabetic dermal matrix contributes to the pathological mechanisms of diabetic skin.[14,15] However, monitoring the induced biochemical or cellular biologic changes of the skin tissue is difficult when the integrity of the biological organization is not damaged.[16]

Confocal Raman microspectroscopy is widely applied as a noninvasive, real-time diagnostic tool in various tissues.[17–20] This technique is used in studies to identify tissues or to compare normal and pathological biological tissues based on the sensitive biochemical and structural information provided by such a spectroscopic technique.[21,22] Confocal Raman microspectroscopy has proven to be an effective biophotonic approach of probing AGEs. Glenn et al.[23] detected the quantitative modification of ocular age-related AGEs in Bruch's membrane

*Address all correspondence to: Hanping Liu, E-mail: liuhp@scnu.edu.cn

1083-3668/2015/$25.00 © 2015 SPIE

dissected from fresh postmortem eye-cups using confocal Raman microspectroscopy. This approach is accurate and nondestructive for predicting ocular aging. Sebag et al.[24] used Raman spectroscopy to investigate the molecular changes of increased nonenzymatic glycation in both the human vitreous specimens obtained from patients with proliferative diabetic retinopathy and the samples of *in vitro* glycated rat tail tendon collagen and demineralized chick bone collagen. Marie et al.[25] applied Raman microspectroscopy to investigate the nonenzymatic glycation process in fibrillar type 1 collagen glycated with glucose or ribose of different levels *in vitro*. They found that Raman spectroscopy is clearly correlated with the accumulation of fluorescent AGE. Therefore, Raman microspectroscopy is proven to be well adapted to highlight the effect of nonenzymatic glycation directly on collagen.

Detection of AGE contents has not been conducted in collagen fibrils from T2D mouse models. In this study, confocal Raman microspectroscopy was used to implement the glycation probe of the collagen scaffolds derived from the dermal layer of T2D mouse models at different timepoints of diabetes. The collagen scaffolds of diabetic mice were obtained using the decellularized dermal matrix, which removes the epidermis layer, subcutaneous tissue, and cells in the dermis, leaving only the collagen fibrils. The vibrational spectroscopic technique, which is a label-free, direct, rapid, and nondestructive approach, was then applied to explore the effects of nonenzymatic glycation on skin collagen of T2D mouse models. Raman signals between the regions of 700 and 1700 cm^{-1} were selected in the analysis of our study because they have been proven to be the fingerprint regions for collagen feature changes by previous studies.

2 Materials and Methods

2.1 *Animals and Type 2 Diabetes Induction*

All experimental procedures were approved by the Ethical Committee for Animal Experiments of South China Normal University. Institute of cancer research (ICR) mice, which are considered the optimal animals for inducing T2D, were selected as the experimental animals. Eight-week-old male ICR mice weighing approximately 30 g were purchased from Guangdong Medical Laboratory Animal Center. Each mouse was housed in a cage with an alternating 12:12 h of light/dark cycle at an ambient temperature of 22°C to 25°C. After adaptive breeding for 5 days, mice were fed with a high-fat diet for 4 weeks. Their diet consisted of 45% fat, 35% carbohydrate, and 20% protein, as well as essential elements to induce T2D with insulin resistance[26] Mice were fasted for 12 h with free access to water and then injected intraperitoneally with streptozocin (STZ, 60 mg/kg; Sigma, United States), a cytotoxic agent for pancreatic β-cells, for 3 days to induce T2D.[27] At 3 days after injection, the fasting body weight (FBW; after 12 h) was measured and fasting blood glucose (FBG; after 12 h) in the tail venous blood was assessed by using a glucose meter (Accu–Chek Active; Roche Diagnostics Brazil Ltd, Brazil). From this point, FBG and FBW were measured every week, and non-FBG was also measured every morning until the end of the experiment. Animals with FBG values of $\geqq$11.1 mmol/L and that exhibited typical clinical polydipsia, polyuria, and weight loss were considered T2D mice.[28,29]

2.2 *Preparation of Collagen Scaffolds*

Fresh mouse skin was obtained from the dorsum and abdomen of ICR mice after anesthesia, and hair was removed. The subdermal fat tissue was excised, and the skin samples were cut into rectangular pieces with dimensions $10 \times 10 \times 3$ mm. The pieces were immersed in 0.25% dispase solution (Aoboxing, Beijing, China) at 4°C for 48 h to remove the epidermis and then extensively washed three times in distilled water. Subsequently, the pieces were incubated in 0.3% Triton X-100 solution with continuous stirring at room temperature for 48 h and then in 0.25% trypsin solution at 4°C for 2 h to remove cells in the dermal structure. The resulting dermal matrix was thoroughly rinsed three times in sterile phosphate buffer solution (PBS) at 4°C for 15 min each. Finally, the packed collagen scaffolds were stored in sterile distilled water at 4°C after being sterilized in 70% ethanol for 2 h.[30–33]

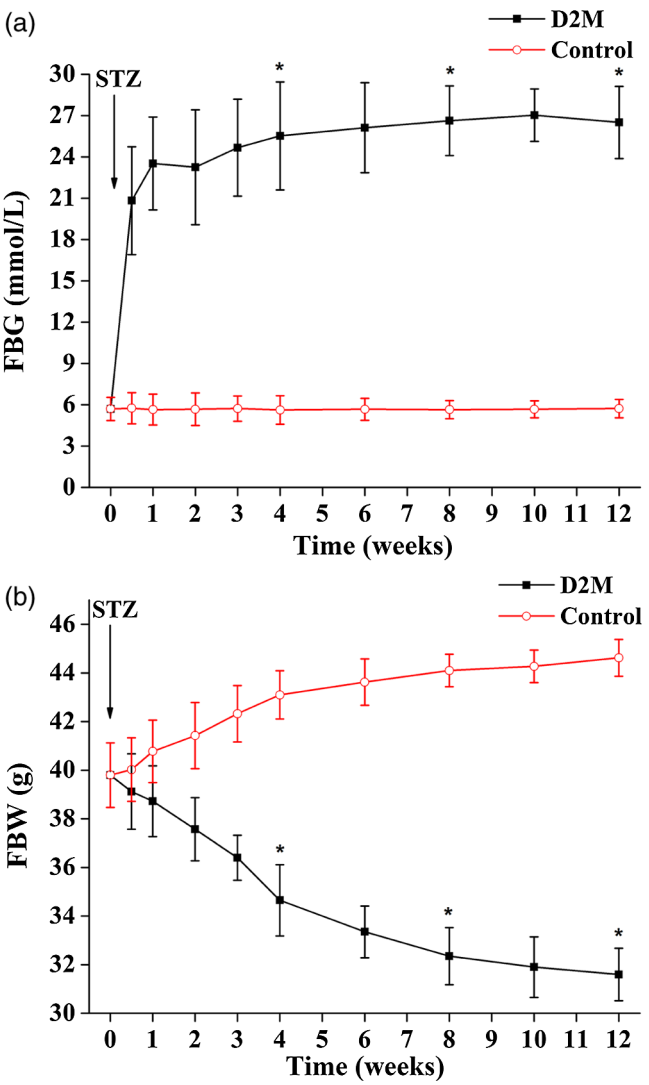

Fig. 1 (a) Average fasting blood glucose (FBG) levels from 0 to 12 weeks ($n = 5$/group). At 0 day, the mice were injected with streptozocin (STZ). (b) Average fasting body weight (FBW) levels from 0 to 12 weeks ($n = 5$/group). At 0 day, the mice were injected with STZ. Compared with the control group at the same time, $^*P < 0.05$.

2.3 *Immunofluorescence Analysis*

Anti-AGE antibody was measured to quantify the glycation levels in the glycated collagen from T2D mice. For immunofluorescence detection, 5-μm paraffin sections of collagen scaffolds were placed in citrate buffer (pH 6.0) inside a steamer for 10 min, blocked by incubation with peroxide block and normal goat serum (Beyotime, Shanghai, China), and incubated with primary anti-AGE antibody (1:400, ab23722; Abcam, Hong Kong) at 4°C overnight. The sections were washed in PBS, and Texas Red®-labeled secondary goat anti-rabbit Ig G-TR (1:100, sc-2780; Santa Cruz Biotechnology, United States) was applied at room temperature for 2 h. All slices were stained with 4',6-diamidino-2-phenylindole (Sigma) for 15 min to display the nuclei. Slice images were obtained using a confocal laser-scanning microscope (710 NLO; Carl Zeiss, Jena, Germany).

2.4 *Confocal Raman Microspectroscopy of Collagen Scaffolds*

The specimens of collagen scaffold were cut into 50-μm thick sections using a Leica CM 1950 cryostat (Leica, Germany). The Raman spectra were directly recorded on collagen scaffolds without further preparation by Renishaw (Renishaw Inc., New Mills) via Raman microspectroscopy system equipped with a 300-mW near-infrared diode laser at a wavelength of 785 nm semiconductor laser for excitation. The laser beam of approximately 15 mW was focused on the sample surface by a 50× objective lens of a Leica DM2500 microscope (Leica, Germany). Experiments were performed using a microscope in a backscattering geometry, where the scattering light was collected inside the cone, defined by the objective. The spectra were recorded with a resolution of 1 cm^{-1} in the range of 700 to 1700 cm^{-1} and collected with 5 s exposure time and three accumulations. All the data were collected under the same conditions. The raw spectra acquired from the collagen scaffolds in the range of 700 to 1700 cm^{-1} represented a combination of prominent autofluorescence, weak Raman scattering signals, and noise. Therefore, baseline correction was carried out by using a modified third-order polynomial fitting followed by smoothing.

2.5 *Statistical Analysis*

All measurements were performed in triplicate sections from each sample. Data preprocessing consisted of three steps: removal of spectra containing cosmic rays, background subtraction, and normalization. Normal distribution of the fluorescence intensity and their homogeneity of variance were analyzed by the Shapiro–Wilk test and Levene's test, respectively. Differences in fluorescence intensity at different timepoints were compared using one-way independent ANOVA and posthoc procedures for multiple comparisons. A Pearson correlation was used to measure the strength of the relationships between Raman intensity and fluorescence intensity of AGEs. All statistics were performed using the Statistical Package for Social Science (SPSS 20, SPSS Inc., Chicago, Illinois). All tests were two-tailed, and $P < 0.05$ was considered statistically significant.

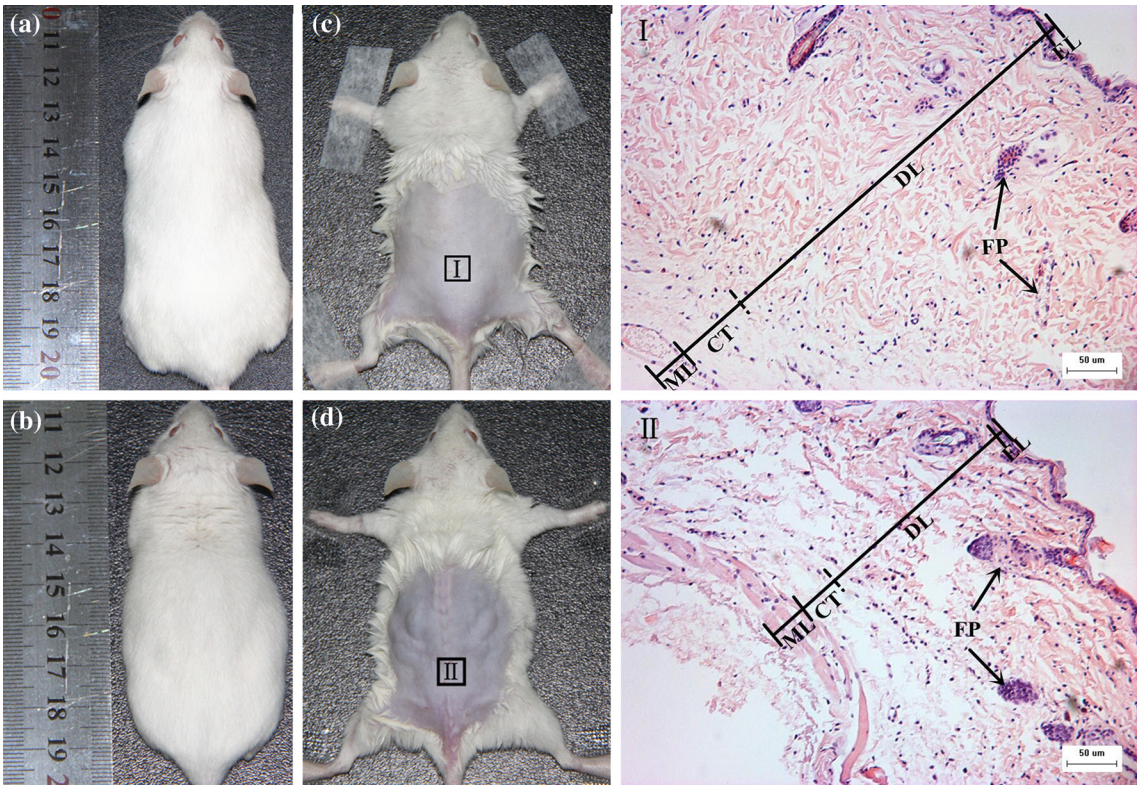

Fig. 2 (a) Appearance of control mouse. (b) Appearance of diabetic mouse. (c) Image of the body part of control mouse without hair. (I): skin hematoxylin-eosin (H and E) image of the control mouse; (d) image of the body part of diabetic mouse without hair. (II): Skin H and E image of the diabetic mouse. Epidermal layer (EL), dermis layer (DL), connective tissue (CT), muscular layer (ML), and folliculus pili (FP) inserted in the dermis are shown from the epidermis to subcutaneous. Scale bar = 50 μm.

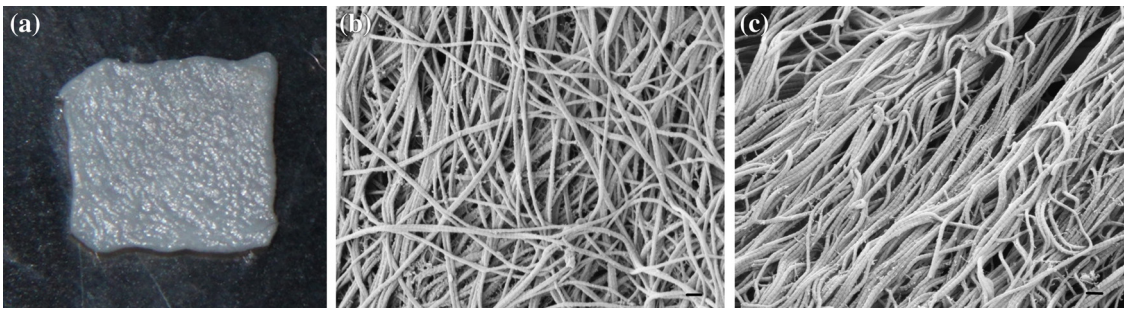

Fig. 3 (a) Image of collagen scaffolds. (b) Scanning electron microscopy (SEM) of collagen scaffold of the control mouse. (c) SEM of collagen scaffold of the diabetic mouse. Electron microscope magnifications of both (b) and (c) are 50000×, and the extra high tension is 5 kV. Scale bar = 200 nm.

3 Results

3.1 *Physiological Characteristics of STZ-Treated Type 2 Diabetes Mice*

To examine whether T2D mice were successfully induced by STZ injection, we observed the behavior and measured the FBW and FBG for 3 days and every week after STZ injections of the control and diabetic mice. The T2D mice exhibited typical clinical symptoms, such as cachexia, polydipsia, and polyuria. Fig. 1(a) shows the average FBG levels of the control and diabetic mice from 1 to 12 weeks after SZT injections. The T2D mice had higher FBG values than the control mice ($P < 0.05$). The FBG levels of the diabetic mice significantly increased during 1 week after STZ injections and nearly reached 25 mmol/L during the whole experiment. All the diabetic levels were above 11.1 mmol/L, which is the standardized criterion for the FBG levels of the diabetic mouse models. However, the FBG levels of the control mice were stable at nearly 5 mmol/L. The average FBW levels of the control and diabetic mice from 1 to 12 weeks are shown in Fig. 1(b). The FBW levels of the diabetic mice significantly decreased during 1 week after STZ injections and reached approximately 32 g in the following experiment compared with those of the control mice ($P < 0.05$). However, the FBW levels of the control mice were stable at nearly 42 g in the following experiment.

Numerous differences were observed in the mice after 9 weeks of diabetes, especially the morphological variations of the skin. Figures 2(a) and 2(b) show that the diabetic mice were smaller and weaker with withered hair ($n = 20$/group). The diabetic mice were about 10.5 cm long, while the control ones were only about 9 cm long. Figures 2(c) and 2(d) show that no significant pathological changes were observed in the skin of both the control and diabetic mice, but the diabetic skin was thinner than the normal skin with reduced elasticity. Figures 2(I) and 2(II) show that the number of the diabetic epidermal cells decreased. Moreover, the cell layer was less clear and lacked a multilayer arrangement. The skin collagen became atrophic, swollen, and degenerated, which were considered the major changes of histology caused by AGEs. The subcutaneous fat also exhibited progressive atrophy or even disappearance and was difficult to distinguish from dermis collagen.

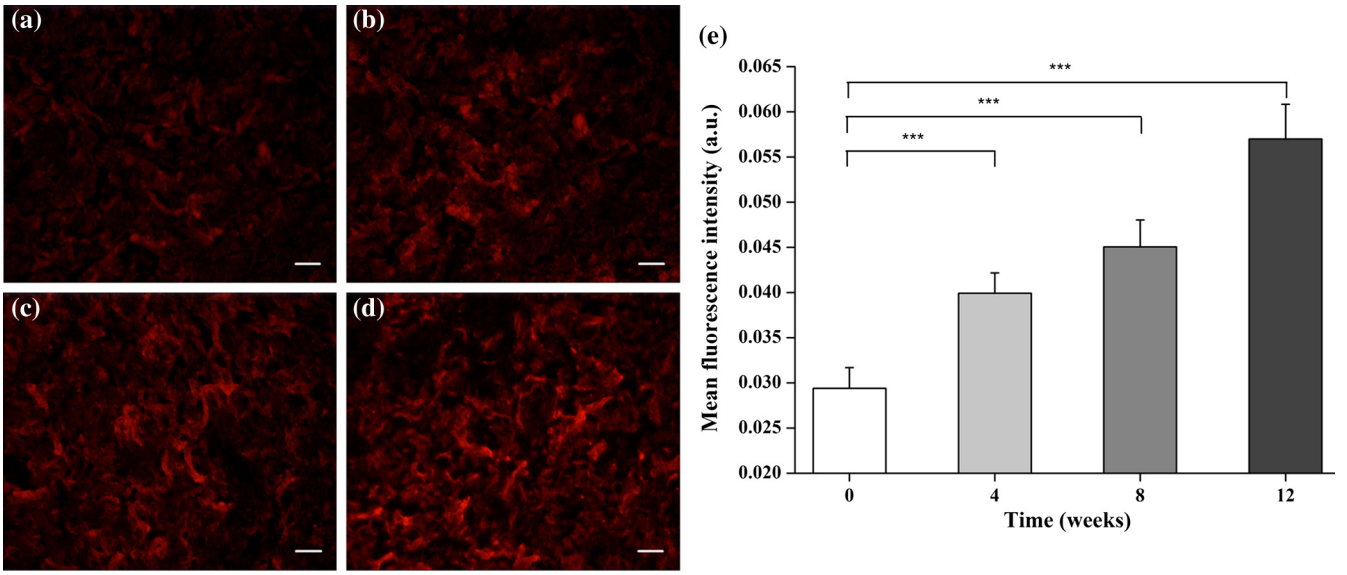

Fig. 4 Immunofluorescence images of collagen advanced glycation end products (AGEs) from type 2 diabetic (T2D) mice at different timepoints. (a) Collagen AGEs of 0 week; (b) 4 weeks; (c) 8 weeks; and (d) 12 weeks. (e) Mean fluorescence intensity analysis was performed in diabetic collagen AGEs at different timepoints ($n = 3$/group). Values are the mean of three independent experiments (***$P < 0.001$, compared with the 0 week glycated collagen scaffolds from T2D mice, mean ± SEM).

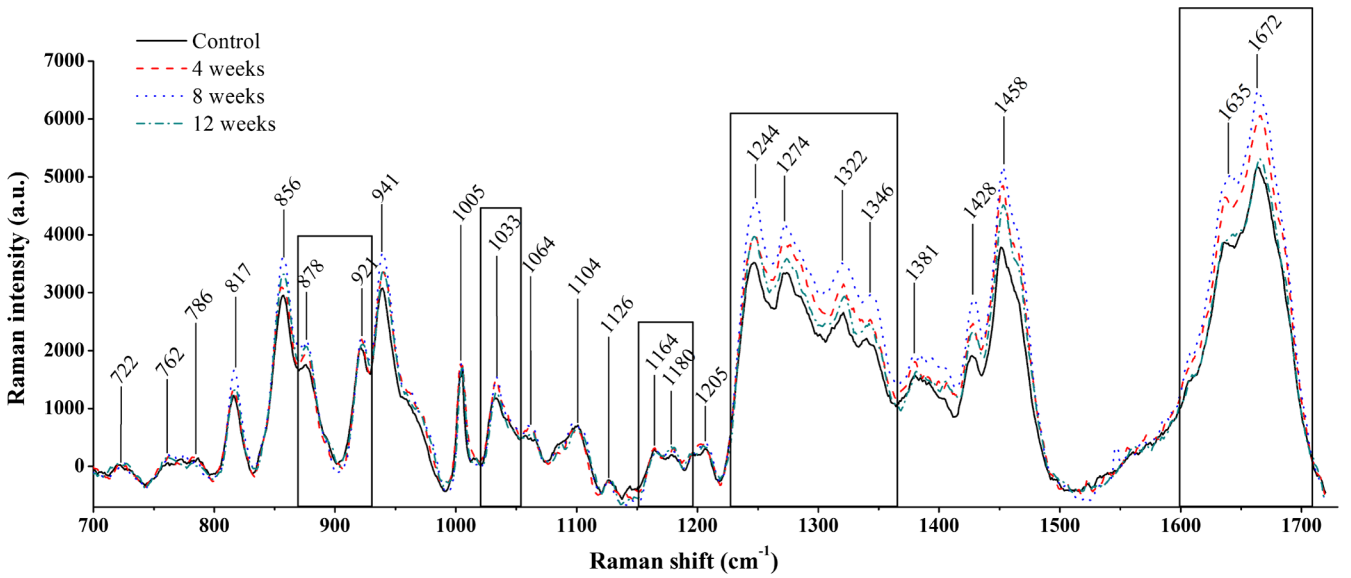

Fig. 5 Raman spectral analysis of glycated collagen scaffolds from T2D mice at different timepoints. Comparisons between Raman spectra of native nonglycated and glycated collagen scaffolds of T2D mice at different timepoints (4, 8, and 12 weeks). Spectra represent means of the three independent measurements and are normalized in the range of 700 to 1700 cm^{-1}. Excitation wavelength, 785 nm; laser power, 15 mw; and laser spot diameter ~1 μm.

3.2 *Characteristics of Collagen Scaffolds*

We prepared the collagen scaffolds by degrading the fresh skin tissue derived from the mice. The collagen scaffolds were porcelain white and transparent. They were soft and resorbable for tissue engineering [Fig. 3(a)]. Collagen fibers in the skin are disassembled into collagen fibrils by decellularizing the dermal matrix. These scaffolds were composed of collagen fibrils without any cells, as shown in the scanning electron microscopy (SEM) images of the control and diabetic mice. The collagen fibrils (diameter < 200 nm) of the control mouse were evenly distributed and extended in all directions [Fig. 3(b)]. However, the structure of the collagen fibrils in the diabetic mice was destroyed. Parts of the diabetic collagen fibrils were arranged in clusters. Also, the horizontal grain and the cross-linking structure of the collagen fibrils in the diabetic mice were more obvious [Fig. 3(c)].

3.3 *Immunofluorescence Assay of Glycated Collagen from Type 2 Diabetes Mice*

In a complementary approach, the accumulation of collagen AGEs was detected by immunofluorescence assay with 5-μm paraffin sections of control and diabetic mice at different

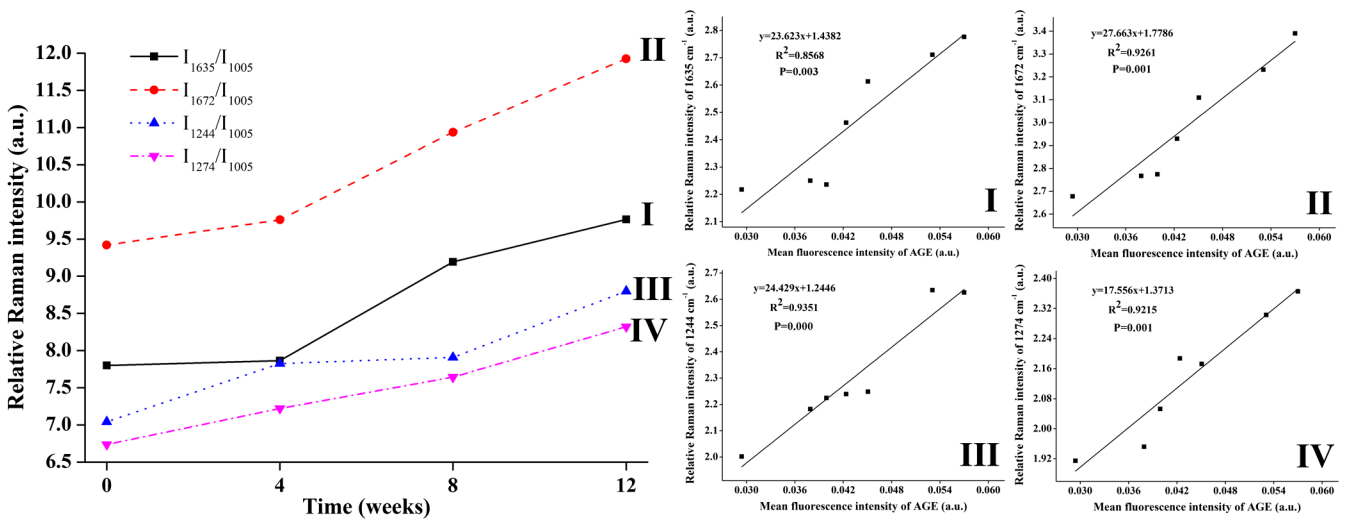

Fig. 6 Analysis of Raman signals of amides I and III residues from glycated collagen scaffolds of 0-, 4-, 8-, and 12-week diabetes. The 1005 cm^{-1} peak corresponded to the Raman signal of Phe group. The 1635 and 1672 cm^{-1} peaks corresponded to the Raman signal of amide I groups, and the 1244 and 1274 cm^{-1} peaks corresponded to the Raman signal of amide III. The ratio of the intensities of each of these peaks (I_{1635}/I_{1005}, I_{1672}/I_{1005}, I_{1244}/I_{1005}, and I_{1274}/I_{1005}) was calculated. (I), (II), (III), and (IV): Correlation analyses between the relative Raman intensity of 1635, 1672, 1244, and 1274 cm^{-1} bands with the mean fluorescence intensity of AGEs.

timepoints. Figures 4(a) to 4(d) display the results of red fluorescence assay of 0, 4, 8, and 12 weeks diabetic glycated collagen scaffolds, respectively, which were emitted by Texas Red®-labeled secondary antibody. Figure 4(e) shows an obvious increase in the red fluorescence of glycated collagen scaffolds as a response of glycation levels. This result indicates that the content of AGEs increased as the diabetic time progressed. The mean fluorescence intensity was calculated by summing the total fluorescence intensity of all measurements and then dividing by the total fluorescent area of measurements.

3.4 *Confocal Raman Microspectroscopic Analysis of Collagen Scaffolds*

The samples were analyzed by confocal Raman microspectroscopy to determine the differences of molecular groups between the control and diabetic collagen scaffolds. Each sample had three slices, and each slice had three spots; that is, nine spots were detected by confocal Raman microspectroscopy for one sample. The mean Raman spectra of the spots on each specimen are shown in Fig. 5, exhibiting the characteristic spectral features with associated band assignments (Table 1).

The peak of 1005 cm^{-1} (assigned to Phe groups) remained highly constant upon glycation. The ratio intensities ($I_{peak\ of\ interest}/I_{1005}$) were calculated for the peak of interest. Amide I (1635 and 1672 cm^{-1}) and amide III (1244 and 1274 cm^{-1}) bands did not exhibit position changes, confirming the conservation of the triple-helix structure of collagen during glycation. However, as shown in Fig. 6, the intensity of the Raman bands increased upon glycation at these positions, suggesting conformational changes, which may be due to the increase of cross-linking degree of collagen caused by nonenzymatic glycation. The correlation analysis suggested that the spectral maps corresponding to these bands had a high positive correlation with the expression of anti-AGE antibody obtained by immunofluorescence imaging of the same collagen scaffolds as shown in Figs. 6(I) to 6(IV). Furthermore, other important changes in peak intensities were revealed upon glycation, especially for residues of prolines (Pro) and hydroxyprolines (HyPro), which were the second and third aminoacids in the collagen triple-helix composition, respectively. The observed changes are represented in Fig. 7, showing a steady increase of the 921, 1033, and 1346 cm^{-1} (Pro) peaks overtime. The bands of Pro residues in the spectral maps exhibited a high positive correlation with the expression of anti-AGE antibody obtained by immunofluorescence imaging of the same collagen scaffolds as shown in the correlation analyses in Figs. 7(I) to 7(III). However, the 878 and 1180 cm^{-1} (HyPro) peaks had no obvious variety regulation, which suggested that collagen glycation had an excellent priority selectivity of Pro rather than HyPro. These data suggested changes in the amino acid exposure and protein backbone of collagen because of high glucose concentration in T2D mice.

4 Discussion

To date, the common methods used to detect AGEs are high-performance liquid chromatography,[34,35] competitive enzyme-linked immune sorbent assays,[36,37] and immunohistochemistry.[38] Studies prove the accumulation of AGEs on collagen in diabetic skin, but no universally accepted or widely used methods are available to monitor *in vivo* AGEs because their different structures that have not been completely identified,[39] and some are intermediate reactive species of glycation or the oxidation of fatty acids.[40] In this study, the structural differences of glycated collagen at different timepoints were identified using confocal Raman microspectroscopy, which can be used as a label-free biophotonic technique for investigating glycated collagen in diabetic mice. A more comprehensive library of Raman spectra for collagen AGEs is in progress. Our findings are important for monitoring the glycated collagen scaffolds from the diabetic skin of animal models by confocal Raman microspectroscopy.

Studies on nonenzymatic glycation of type 1 collagen extracted from the tendon of nondiabetic mouse tails with glucose or ribose of different levels *in vitro* have been performed by

Table 1 Raman-selected bands (cm^{-1}) and assignments in the range of 700 to 1700 cm^{-1} region of glycated collagen scaffolds from type 2 diabetic (T2D) mice at different timepoints.

Raman shift/cm^{-1}	Tentative assignments
722	γ(C-C)
762	γ(C-C)
786	γ(C-C)
817	γ(C-C)
856	γ(C-C) of Pro
878	γ(C-C) of HyPro
921	γ(C-C) of Pro
941	γ(C-C) of backbone
1005	Phe
1033	Pro
1064	γ(C-N)
1104	γ(C-N)
1126	γ(C-C)
1164	γ(C-C)
1180	HyPro
1205	Phe
1244	amide III
1274	amide III
1322	δ(CH)
1346	CH_2 wagging of Pro
1381	$\gamma(COO^-)$ sym
1428	$\gamma(COO^-)$
1458	C-H bend
1635	amide I
1672	amide I

Abbreviations: γ, stretching vibration; δ, deformation vibration; Phe, phenylalanine; Tyr, tyrosine; Pro, proline; HyPro, hydroxyproline.

Raman microspectroscopy.[27] However, skin collagen contains at least two types of collagen fibers, namely, types 1 and 3. The amount of skin types 1 and 3 collagen fibers remains uncertain, as well as the ratio of type 3 to type 1 fibers.[41] In contrast to previous studies, detection of either type 1 or 3 glycated collagen isolated by glucose or ribose of different levels *in vitro* in this study can reflect the real condition of collagen glycation existing in biological tissues. The glycation process of collagen *in vivo* is a complex process that cannot be easily simulated *in vitro*.[42] Therefore, this study focused on detecting collagen glycation *in vivo* because it is more significant than that *in vitro*.

Skin is a complex tissue that is composed of stratum corneum, epidermal layer, dermis layer, and subcutaneous connective tissue. The components of each layer are different; thus, identifying the collagen for glycated detection by confocal Raman microspectroscopy is difficult. Given this reason, this study adopted the decellularized dermal matrix method to remove the epidermis layer, subcutaneous tissue, and cells in the dermis of the skin. After biological treatment, collagen was retained, thereby eliminating the interferences of noncollagenous components to the Raman spectra. This study is the first to use confocal Raman spectroscopy to detect glycated collagen from T2D mice at different timepoints through the decellularized dermal matrix method. The results showed that the relative Raman intensities of amide I, amide III, and Pro groups increased upon glycation without changes in peak shifts as the diabetes progressed, and exhibited a high positive correlation with the mean fluorescence intensity of AGEs. The results of this study can contribute to the research about the changes of the Raman spectrum for *in vivo* collagen glycation in T2D mice and may provide a new method for detection.

The collagen scaffolds obtained by the decellularized dermal matrix method were potentially important for numerous practical applications, such as in abdominal wall repair,[43] ventral hernia repair,[44] prosthesis-based breast reconstruction,[45] and skin grafts for whole cortex injury.[46] Using confocal Raman microspectroscopy to detect skin collagen scaffolds allowed us to learn more information about the molecular structures of collagen scaffolds, which can lay the foundation for the wide use of collagen scaffolds in the future.

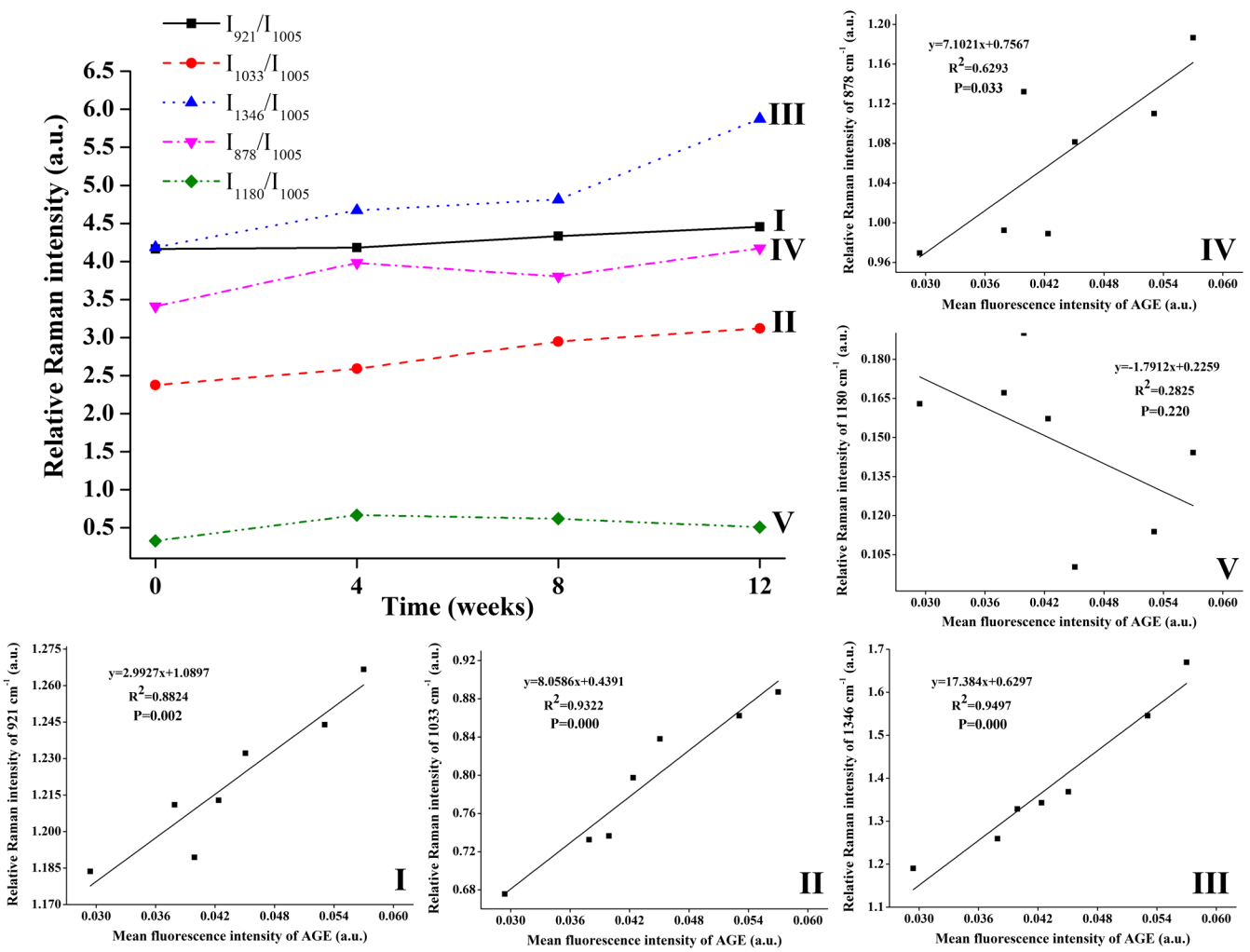

Fig. 7 Analysis of Raman signals from Pro and HyPro residues from glycated collagen scaffolds of 0-, 4-, 8-, and 12-week diabetes. The 1005 cm^{-1} peak corresponded to the Raman signal of the Phe group. The 921, 1033, and 1346 cm^{-1} peaks corresponded to the main Raman signal of the Pro group, and the 878 and 1180 cm^{-1} peaks corresponded to the main Raman signal of the HyPro group. The ratio of the intensities of each of these peaks (I_{1921}/I_{1005}, I_{1033}/I_{1005}, I_{1346}/I_{1005}, I_{878}/I_{1005}, and I_{1180}/I_{1005}) was calculated. (I), (II), (III), (IV) and (V): Correlation analyses between the relative Raman intensity of 921, 1033, 1346, 878, and 1180 cm^{-1} bands with the mean fluorescence intensity of AGEs.

5 Conclusions

We obtained the collagen scaffolds through the decellularized dermal matrix method. AGE immunofluorescent assay and confocal Raman microspectroscopy were applied to obtain the AGE immunofluorescence images and Raman spectra of glycated collagen from diabetic mice at different timepoints. After detailed assignment and analysis of the peaks in the range of 700 to 1700 cm^{-1}, the results revealed that nonenzymatic glycation brought no new spectral peaks or had no shifts of the main amino acid in collagen, but confocal Raman microspectroscopy could detect the differences in the peaks of amide I (1635 and 1672 cm^{-1}), amide III (1244 and 1274 cm^{-1}), and Pro (921, 1033, and 1346 cm^{-1}) from diabetic glycated collagen at different timepoints. The position stability of amide I (1635 and 1672 cm^{-1}) and amide III (1244 and 1274 cm^{-1}) bands confirmed that the triple-helix structure of collagen remained unchanged upon glycation during diabetes. However, the intensity of the aforementioned bands increased upon glycation, suggesting conformational changes, such as skeletal deformation, which may be due to the increase of the cross-linking degree of collagen caused by nonenzymatic glycation in diabetic mice. The HyPro and carbohydrate bands can also be used for monitoring collagen glycation in diabetic mice to some degree. Moreover, the immunofluorescent images can also confirm that collagen glycation in diabetic mice increased as diabetic time progressed. Confocal Raman microspectroscopy is a powerful tool for label-free monitoring of collagen changes caused by nonenzymatic glycation in T2D mice.

Acknowledgments

National Natural Science Foundation of China (No. 81171379) provided funding for this research. This study was also supported by College of Biophotonics of South China Normal University for animal experiments and Raman microcopy detection.

References

1. American Diabetes Association, "Diagnosis and classification of diabetes mellitus," *Diabetes Care* **37**(Suppl), S81–S90 (2014).
2. R. D. Chen and L. Lu, "Nutrition-related metabolic disease-type 2 diabetes mellitus," *Med. J. Chin. People's Armed Police Forces* **2**, 101–104 (2009).
3. A. H. Zhang et al., "Metabolomics in diabetes," *Clin. Chim. Acta* **429**, 106–110 (2014).
4. C. J. Nolan, P. Damm, and M. Prentki, "Type 2 diabetes across generations: from pathophysiology to prevention and management," *Lancet* **378**(9786), 169–181 (2011).
5. A. Negre-Salvayre et al., "Hyperglycemia and glycation in diabetic complications," *Antioxid Redox Sign.* **11**(12), 3071–3109 (2009).
6. N. Ahmed, "Advanced glycation end products—role in pathology of diabetic complications," *Diabetes Res. Clin. Pract.* **67**(1), 3–21 (2005).
7. R. Armando and A. M. Miguel, "Advanced glycation and endothelial functions: a link towards vascular complications in diabetes," *Life Sci.* **76**(7), 715–730 (2004).
8. N. Khan et al., "Ameliorative potential of spironolactone in diabetes induced hyperalgesia in mice," *Yakugaku Zasshi* **129**(5), 593–599 (2009).
9. Z. Ruszczak, "Effect of collagen matrices on dermal wound healing," *Adv. Drug Deliv. Rev.* **55**(12), 1595–1611 (2003).
10. G. Said et al., "Impact of carbamylation and glycation of collagen type I on migration of HT1080 human fibrosarcoma cells," *Int. J. Oncol.* **40**, 1797–1804 (2012).
11. N. C. Avery and A. J. Bailey, "The effects of the Maillard reaction on the physical properties and cell interactions of collagen," *Pathol. Biol. (Paris)* **54**(7), 387–395 (2006).
12. M. Leveriza-Oh, "Diabetes and your skin: protecting your outermost layer," *Diabetes Self Manage.* **23**(4), 1618–2002 (2006).
13. A. Yuen et al., "Methylglyoxal-modified collagen promotes myofibroblast differentiation," *Matrix Biol.* **29**(6), 537–548 (2010).
14. H. J. Liao, Z. Julia, and W. L. Chen, "Cells and tissue interactions with glycated collagen and their relevance to delayed diabetic wound healing," *Biomaterials* **30**(9), 1689–1696 (2009).
15. Y. Niu et al., "Reduced dermis thickness and AGE accumulation in diabetic abdominal skin," *Int. J. Low Extreme Wounds* **11**(3), 224–230 (2012).
16. W. D. Lin et al., "Pathophysiological changes of dermal tissue in diabetic rats and their mechanisms," *J. Tongji Univ. (Med. Sci.)* **22**(22), 7–14 (2012).
17. B. Bodanese et al., "Differentiating normal and basal cell carcinoma human skin tissues *in vitro* using dispersive Raman spectroscopy: a comparison between principal components analysis and simplified biochemical models," *Photomed. Laser Surg.* **28**(1), S119–S127 (2010).
18. A. S. Haka et al., "Diagnosing breast cancer by using Raman spectroscopy," *Proc. Natl. Acad. Sci.* **102**(35), 12371–12376 (2005).
19. C. Krafft and V. Sergo, "Biomedical applications of Raman and infrared spectroscopy to diagnose tissues," *Spectrosc. Int. J.* **20**(5–6), 195–218 (2006).
20. N. Stone et al., "Raman spectroscopy for identification of epithelial cancers," *Faraday Discuss.* **126**, 141–157 (2004).
21. M. Kozielski et al., "Determination of composition and structure of spongy bone tissue in human head of femur by Raman spectral mapping," *J. Mater. Sci. Mater. Med.* **22**(7), 1653–1661 (2011).
22. R. Manoharan, Y. Wang, and M. S. Feld, "Histochemical analysis of biological tissues using Raman spectroscopy," *Spectrochim. Acta Part A.* **52**(2), 215–249 (1996).
23. J. V. Glenn et al., "Confocal Raman microscopy can quantify advanced end product (AGE) modifications in Bruch's membrane leading to accurate, nondestructive prediction of ocular aging," *FASEB J.* **21**(13), 3542–3552 (2007).
24. J. Sebag et al., "Raman spectroscopy of human vitreous in proliferative diabetic retinopathy," *Invest. Ophthalmol. Vis. Sci.* **35**(7), 2976–2980 (1994).
25. G. Marie et al., "Probing non-enzymatic glycation of type I collagen: a novel approach using Raman and infrared biophotonic methods," *BBA Gen. Subjects* **1830**(6), 3525–3531 (2013).
26. M. T. Nowicki et al., "Renal and hepatic transporter expression in type 2 diabetic rats," *Drug Metab. Lett.* **2**(1), 11–17 (2008).
27. A. A. Like and A. A. Rossini, "Streptozotocin-induced pancreatic insulitis: new model of diabetes mellitus," *Science* **193**(4251), 415–417 (1976).
28. N. Xie et al., "Advancement in diabetes animal models," *J. Xinxiang Med. Coll.* **24**(6), 629–632 (2007).
29. N. M. Argolo Neto et al., "Role of autologous mesenchymal stem cells associated with platelet-rich plasma on healing of cutaneous wounds in diabetic mice," *Clin. Exp. Dermatol.* **37**(5), 544–553 (2012).
30. R. N. Chen et al., "Process development of an acellular dermal matrix (ADM) for biomedical applications," *Biomaterials* **25**(13), 2679–2686 (2004).
31. X. J. Zhang et al., "Expansion and delivery of human fibroblasts on micronized acellular dermal matrix for skin regeneration," *Biomaterials* **30**(14), 2666–2674 (2009).
32. L. P. Ge, S. Q. Zheng, and H. Wei, "Comparison of histological structure and biocompatibility between human acellular dermal matrix (ADM) and porcine ADM," *Burns* **35**(1), 46–50 (2009).
33. C. D. Richters et al., "Development of a dermal matrix from glycerol preserved allogeneic skin," *Cell Tissue Bank.* **9**(4), 309–315 (2008).
34. D. R. Sell and V. M. Monnier, "End stage renal disease and diabetes catalyse the formation of a pentose-derived cross-link form aging human collagen," *J. Clin. Invest.* **85**, 380–384 (1990).
35. P. Papanastasiou et al., "Immunological quantification of AGE's in serum of patients on haemodialysis or peritoneal dialysis," *Kidney Int.* **46**, 216–222 (1994).
36. S. Sugiyama et al., "Advanced glycation end-products in diabetic nephropathy," *Nephrol. Dial. Transplant.* **11**(S5), S91–S94 (1996).
37. G. Munch et al., "Determination of advanced glycation end products in serum by fluorescence spectroscopy and competitive ELISA," *Eur. J. Clin. Chem. Clin. Biochem.* **35**(9), 669–677 (1997).

38. T. Soulis et al., "Advanced glycation end-products and their receptors co-localise in rat organs susceptible to diabetic microvascular injury," *Diabetologia* **40**(6), 619–628 (1997).
39. T. Mitsuhashi et al., "Standardising the immunological measurement of advanced glycation end products using normal human serum," *J. Immunol. Methods* **207**(1), 79–88 (1997).
40. R. Singh et al., "Advanced glycation end products: a review," *Diabetologia* **44**(2), 129–146 (2001).
41. M. Savvas et al., "Type III collagen content in skin of postmenopausal women receiving oestradiol and testosterone implants," *Br. J. Obstet. Gynaecol.* **100**, 154–158 (1993).
42. R. G. Paul and A. J. Bailey, "Glycation of collagen: the basis of its central role in the late complications of ageing and diabetes," *Int. J. Biochem. Cell Biol.* **28**(12), 1297–1310 (1996).
43. N. K. Burns et al., "Non-cross-linked porcine acellular dermal matrices for abdominal wall reconstruction," *Plast. Reconstr. Surg.* **125**(1), 167–176 (2010).
44. K. T. Campbell et al., "Human versus non-cross-linked porcine acellular dermal matrix used for ventral hernia repair: comparison of *in vivo* fibrovascular remodeling and mechanical repair strength," *Plast. Reconstr. Surg.* **127**(6), 2321–2332 (2011).
45. A. S. Liu et al., "Postoperative complications in prosthesis-based breast reconstruction using acellular dermal matrix," *Plast. Reconstr. Surg.* **127**(5), 1755–1762 (2011).
46. D. J. Wainwright and S. B. Bury, "Acellular dermal matrix in the management of the burn patient," *Aesthetic Surg. J.* **31**(7 Suppl), S13–23 (2011).

Panpan Shi received her BS degree in biotechnology from Beifang University of Nationality in 2012. She is now studying at the College of Biophotonics, South China Normal University. Her research interest is the stem cells for diabetic wound healing.

Hanping Liu is an associate professor at South China Normal University. He received his BS and MS degrees in traditional Chinese medicine from Shaanxi University of Chinese Medicine in 1996 and 2001, respectively, and his PhD degree from Shanghai University of Traditional Chinese Medicine in 2004. His current research interests include biomedical photonics and stem cell research for skin regeneration.

Xiaoyuan Deng is an associate professor at South China Normal University. She received her BS degree from Wuhan Automotive Polytechnic University in 1989, her MS degree from Beijing Institute of Technology in 1994, and her PhD degree from Chinese Academy of Sciences in 1998. Her research interests include the application of nonlinear optical imaging in biological tissue.

Ying Jin is an associate professor at South China Normal University. He received his BS and MS degrees in biology from Inner Mongolia University in 1989 and 1992. His current research includes embryo engineering and biomedical photonics.

Qiannan Wang received her BS degree from Henan University of Science and Technology in 2011. She is now studying at the College of Biophotonics, South China Normal University.

Hao Liu received her BS degree in biotechnology from the University of South China in 2013. She is now studying at the College of Biophotonics, South China Normal University.

Maosheng Chen received his BS degree in biotechnology from Liaoning University in 2013. He is now studying at the College of Biophotonics, South China Normal University.

Xue Han received her BS degree in optical information science and technology from Shandong University of Technology in 2013. She is now studying at the College of Biophotonics, South China Normal University.